2024 IEEE/RSJ International Conference on Intelligent Robots and Systems (IROS)
October 14-18, 2024. Abu Dhabi, UAE

Thermal Ablation Therapy Control with Tissue Necrosis-driven Temperature Feedback Enabled by Neural State Space Model with Extended Kalman Filter

Ryo Murakami[1], Satoshi Mori[2] and Haichong K. Zhang[3]

***Abstract*— Thermal ablation therapy is a major minimally invasive treatment. One of the challenges is that the targeted region and therapeutic progression are often invisible to clinicians, requiring feedback provided in numerical information or imaging. Several emerging imaging modalities offer visualization of the ablation-induced necrosis formation; however, relying solely on necrosis monitoring can result in tissue overheating and endangering patients. Some of the necrosis monitoring modalities are known for their capabilities in temperature sensing, but the principles on which they are based have several limitations, such as sensitivity to the tissue motion and their environment. In this study, we propose a necrosis progression-based temperature estimation technique as an added safety feature for avoiding overheating. This model-based method does not require additional sensing hardware. It is designed to work as an independent estimator or a complimentary estimation component with other thermometers for improved robustness. For this objective, the Neural State Space model is used to approximate the ablation therapy, whose theoretical models involve nonlinear partial differential equations. Then, the Extended Kalman Filter is designed based on the model. The simulation study shows the estimation module robustly estimates the tissue temperature under several types of noise. The maximum estimation error observed before terminating ablation was around 1 °C, and the desired safety feature was successfully demonstrated. The estimator is expected to be used in a variety of necrosis monitoring modalities to guarantee more precise and safer treatment. More ambitiously, the architecture with the Neural State Space model and Extended Kalman Filter is generalizable to other medical/biological procedures involving nonlinear and patient/environment-specific physics and even to procedures having no reliable theoretical models.**

I. INTRODUCTION

Thermal ablation therapy is frequently used in today's clinical settings as one of the major techniques of minimally invasive intervention. The low invasiveness addresses several challenges that conventional open surgeries are facing. For example, it allows access to deep or sensitive areas while minimizing the damage to the surrounding important regions such as nerves and blood vessels. In addition, its limited physical burden can result in much shorter hospitalization and provide vulnerable patients such as elderly people with proactive treatment options; otherwise, the disease would be just managed, not treated. Brain tumor ablation is one of the examples to which the ablation therapy is widely applied [1].

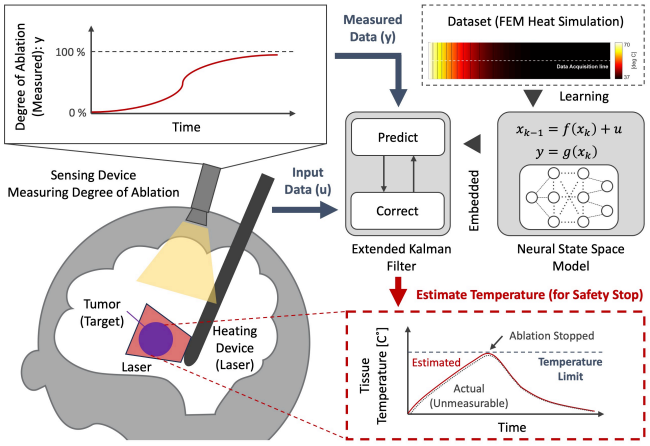

Fig. 1. Concept drawing illustrating developed safety feature for thermal ablation control; The temperature safety feature is expected to turn off the ablation based on the estimated temperature. The temperature estimation will be achieved using the Extended Kalman Filter designed based on the Neural State Space model, which is prepared through the learning of the FEM-based simulation dataset.

Although ablation therapy provides significant benefits in several aspects, one of the challenges of this technique is that the ablation applicator, the targeted region, and therapeutic progression are usually invisible to clinicians and the therapy needs to be performed under feedback provided as numerical or visual information and in most cases, RGB cameras are not in the options due to the limited space and blood filled in the space. Therefore, it is challenging to visually monitor how the tissue reacts with the heat, resulting in feed-forward-like ablation protocol in some cases such as cardiac ablation for atrial fibrillation (AF). In fact, it is well-known that the recurrence rate of AF after ablation therapy is quite high [2], which implies the ablation is not supplied as expected.

In order to provide a feedback-control capability during the thermal ablation procedure, several approaches have been introduced. Direct necrosis monitoring-based feedback control (NFB) is one of the examples and it is expected to provide more precise and safer ablation than the techniques available today in clinical settings [3]. The NFB control is based on the direct monitoring of the heat-induced necrosis formation, not monitoring the tissue temperature and estimating the necrosis formation based on the temperature and the

[1]Ryo Murakami is with Department of Robotics Engineering, Worcester Polytechnic Institute, 50 Prescott St., Worcester MA, The United States rmurakami@wpi.edu
[2]Satoshi Mori is with No Affiliations, Ehime, Japan wald.s1t5@gmail.com
[3]Haichong K. Zhang is with Department of Biomedical Engineering, Robotics Engineering, and Computer Science Engineering, Worcester Polytechnic Institute, 50 Prescott St., Worcester MA, The United States hzhang10@wpi.edu

assumed necrosis formation model. Therefore, differentiation of the tissue characteristics is required and several imaging modalities such as ultrasound (US) [4]–[6] and photoacoustic (PA) imaging [7]–[9] have been used and their capabilities have been demonstrated.

Although the NFB control can theoretically provide accurate ablation, NFB alone can cause a different issue: the induced heat can be too high and endanger patients. One of the typical examples is the "steam-pop", which is reported in the cardiac ablation domain and can cause cardiac perforation and tamponade, which is a life-threatening condition [10]. It is analyzed that the steam-pop occurs when the actual tissue temperature exceeds 100 °C [11]. Even in the case in which the cardiac ablator has a temperature sensor at the electrode, it is known that there is a discrepancy between the displayed temperature and the actual tissue temperature, which makes the prediction of the steam-pop challenging [12]. Also, in brain ablation, it is reported that the ablation control software has the feature to automatically deactivate ablation when the temperature exceeds the predefined limit temperature in a certain area [13]. These examples imply the importance of the safety feature based on the actual tissue temperature for patient safety even when the NFB control is used as the primary control approach.

Whereas one of the direct solutions to this issue is to add a thermometer, several challenges exist in a variety of aspects such as cost and reliability. For example, intraoperative magnetic resonance imaging (iMRI) is the existing reliable thermometer for ablation, but it is highly expensive and not installed in many hospitals. Moreover, iMRI provides strict restrictions on the materials to use in the room [14]. As a different example, some cardiac ablation devices have a temperature sensor at the electrode, but it is not regarded as a reliable thermometer for actual tissue temperature monitoring [15] and it does not access the temperature inside the tissue.

Another challenge is that although some necrosis sensing modalities such as the US and PA are also capable of temperature monitoring [16], [17], there are several limitations in temperature sensing due to the physics on which they are based. For example, the PA thermometer is mainly based on the phenomenon called the photoacoustic effect. The effect is affected not only by target temperature but also by other factors such as material properties, ambient temperature, sensor position, and light source stability, which makes this approach sensitive to the environment, requiring well-controlled conditions [18], [19]. The US-based thermometer mainly relies on shifting in acoustic properties such as attenuation, speed of sound, and backscattered energy. Nonetheless, several limitations such as its high sensitivity to tissue motion are reported [20], [21], which makes the US-based thermometer challenging to use for clinical purposes.

Given the challenges above, we aim to propose a necrosis progression-based tissue temperature estimation technique as an added safety feature for avoiding overheating. This model-based method does not require any additional sensing hardware. It is designed to work even if the necrosis monitoring modality does not have temperature monitoring capability, and if the necrosis monitoring modality has temperature monitoring capability, the proposed approach can be used as another variable to provide for improved robustness. Since the idea is based on the necrosis progression, the principle is expected to be compatible with all necrosis monitoring modalities.

As a technical approach toward this objective, we choose to use the idea of the observer because the tissue temperature can be formulated in the context of state estimation in control engineering. Since one of the strengths of control engineering is its generality and resulting compatibility with a wide variety of applications, ablation therapy should be dealt with under the generalized field of control theory. In fact, some medical-related domains such as neuroscience have actively used control theory to tackle their challenges [22], [23]. Based on Fig. 2, necrosis formation can be seen as the measured output from the system, and the tissue temperature can be categorized as one of the internal states of the system.

One of the challenges in applying control engineering to medicine/biology-related processes is to have an appropriate model, and even if the models are derived, they can be highly nonlinear and challenging to solve efficiently [24]. Thus, the neural state space (NSS) model is selected in this study to formulate the corresponding state space model because the NSS model is known for its usefulness particularly when linear models fall short due to the non-linearity of the system [25]. As an observer, the Extended Kalman Filter (EKF) is selected for its computational efficiency [26] and simplicity.

In this paper, we propose a temperature estimation technique based on necrosis formation (Fig. 1). The estimator enables providing a safety feature automatically terminating ablation before the tissue temperature exceeds the safety limit. For this objective, the NSS model is used to approximate the ablation therapy, whose theoretical models involve nonlinear partial differential equations. As an observer, the EKF is designed based on the NSS model to estimate the tissue temperature. The performance of both the NSS model and the EKF-based state estimation is evaluated as an independent temperature estimator and the temperature safety feature is demonstrated in the simulation environment.

II. MATERIALS AND METHODS

A. Bioheat Transfer Equation

The heat transfer within biological tissue is modeled using Pennes' formula, as depicted in Equation 1 [27], [28].

$$\rho c_t \frac{dT}{dt} = \nabla \cdot k \nabla T - \omega_b c_b (T - T_b) + Q \tag{1}$$

here, ρ, c_t, and k represent the density (kg/m^3), specific heat capacity (J/kg/°C), and thermal conductivity (W/m/°C) of tissue, respectively. T indicates the temperature at the specific point of interest (°C) and T_b is the temperature of blood (°C). ω_b is the rate of blood perfusion (kg/m^3/s), c_b represents the specific heat capacity of blood (J/kg/°C), and Q encapsulates the heat from other heat sources (W/m^3). For the purpose of simplification in this study, the components, Q and $\omega_b c_b (T - T_b)$ have been omitted.

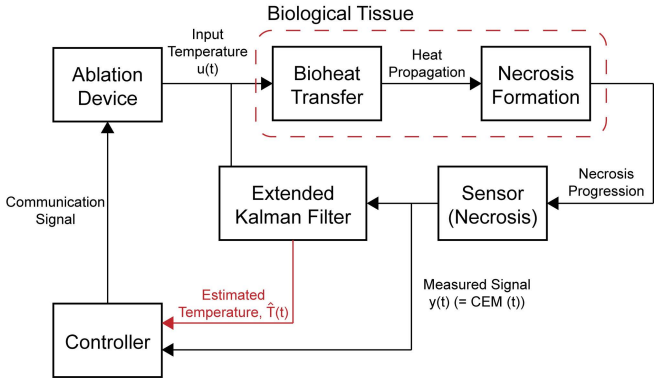

Fig. 2. Block diagram for the temperature estimator and the safety feature; The ablation device is assumed to generate and deliver heat to the biological tissue based on the communication signal from the controller. The applied heat propagates through the tissue and the heat-induced necrosis is formed by the accumulated heat dose. The necrosis progression is monitored with the necrosis sensor. The implemented Extended Kalman Filter embedding the Neural State Space model takes the measured necrosis progression and the ablation temperature to provide the estimated tissue temperature $\hat{T}$ to the controller so that the controller can automatically turn off the ablation device as the desired safety feature.

B. Necrosis Formation Model

The formation of heat-induced tissue necrosis generally depends on the duration and intensity of thermal exposure. Various models have been proposed to describe this phenomenon, one of which is the Arrhenius formulation [29]. Our investigation employs the model formulated by Sapareto and Dewey, as illustrated by Equation 2 [29].

$$\mathrm{CEM43} = \sum_{t=0}^{t=\mathrm{final}} R^{(43-T_t)}\Delta t, \begin{cases} R{=}0.25 \text{ for } T{<}43^{\circ}\mathrm{C} \\ R{=}0.50 \text{ for } T{\geq}43^{\circ}\mathrm{C} \end{cases} \tag{2}$$

In this context, CEM43 denotes the total equivalent number of minutes at 43 °C, Δt and T represent the time interval in minutes and the mean temperature during the interval, respectively. R is the factor compensating the temperature deviation from the temperature threshold, which is set at 43 °C in this particular study [29]. To determine whether sufficient ablation is provided, a threshold value for CEM, 70, is used in this study as the value was used in other brain-related ablation research [30].

C. State Space Model

1) Neural State Space Model: In this study, the state variable is defined as follows:

$$\boldsymbol{x}[k] = \begin{bmatrix} T[k, d_{\mathrm{target}}] \\ \mathrm{CEM}[k, d_{\mathrm{target}}] \end{bmatrix} \tag{3}$$

where, k is the discrete time step, and d_{target} represents the depth of the targeted area of tissue ($\boldsymbol{x} \in \Re^{2\times 1}$ and $y, u \in \Re$). Since it is assumed that CEM is observed as the measured output, the state and output functions have the following forms for discrete-time state-space systems:

$$\boldsymbol{x}[k+1] = \boldsymbol{f}(\boldsymbol{x}[k], u[k]) \tag{4}$$

$$y[k] = \begin{bmatrix} 0 & 1 \end{bmatrix} \cdot \boldsymbol{x}[k] \tag{5}$$

Here, the state function $\boldsymbol{f}$ will be approximated by using a neural network [25]. In this study, the System Identification Toolbox provided in MATLAB software (MATLAB, The MathWorks, Inc., Massachusetts, United States) is used for the NSS-related implementations.

2) Neural Network (Multi-Layer Perceptron): A multi-layer perceptron (MLP) is used within the NSS model (Fig. 3). The network has three fully connected layers, which have 32, 64, and 32 nodes, respectively. There are two inputs assumed ($\boldsymbol{x}[k]$ and u[k]) and one output ($d\boldsymbol{x}[k]$).

D. Extended Kalman Filter

The EKF is selected in this study to estimate the temperature during ablation therapy. EKF is an algorithm used for estimating the state of nonlinear dynamic systems from a series of incomplete and noisy measurements. Unlike the standard Kalman Filter, which is optimal for linear systems with Gaussian noise, the EKF is designed to handle nonlinearities in the system or measurement equations by linearizing around the current estimate [31]. Although some other algorithms such as the Unscented Kalman Filter (UKF) [32] and Particle Filter (PF) [33] can provide better performance when a system has a high nonlinearity, the simplicity and the computational efficiency of EKF make it one of the popular advanced Kalman Filters for nonlinear systems [26], [32].

E. Simulation Environment & Conditions

The layout of the finite element method (FEM) environment is depicted in Fig. 4 (a), which has a rectangular model with dimensions of 20 mm by 4 mm. The left boundary represents the surface of the body, and the ablation device is assumed to be mounted on this surface. The device offers a variable temperature ranging from 37 °C to 70 °C [3]. The tissue temperature and the resulting necrosis formation are evaluated along the horizontal line in the middle of the model [3]. The parameters used in the simulation are summarized in Table I. Fig. 4 (b) displays an example of the simulation, highlighting the progression of heat from the left boundary. The FEM calculations are executed on the MATLAB platform and its Partial Differential Equation Toolbox (MATLAB, The MathWorks, Inc., Massachusetts, United States).

TABLE I
GLOBAL PARAMETERS FOR FEM SIMULATION (HUMAN BRAIN)

Symbols	Description	Value	Unit
T_{duration}	Simulating duration	500	Second
T_{step}	Time step	1	Second
k	Heat conductivity [34]	0.51	W/(m·°C)
ρ	Density [34]	1046	kg/m^3
c_p	Heat capacity [34]	3630	J/(kg·°C)
T_b	Body Temperature (Human)	37	°C
$T_{a(\max)}$	Maximum ablation temperature	70	°C
$T_{a(\min)}$	Minimum ablation temperature	37	°C

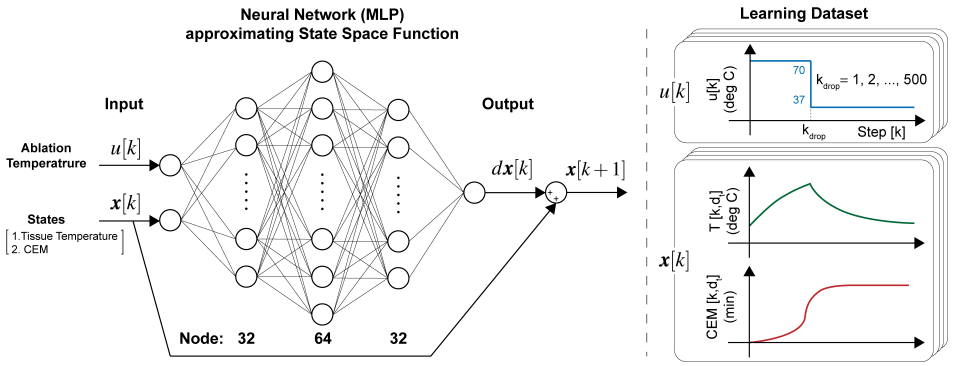

Fig. 3. (Left) Designed neural network (MLP) approximating state space function, (Right) Schematics of learning dataset generated in FEM simulation.

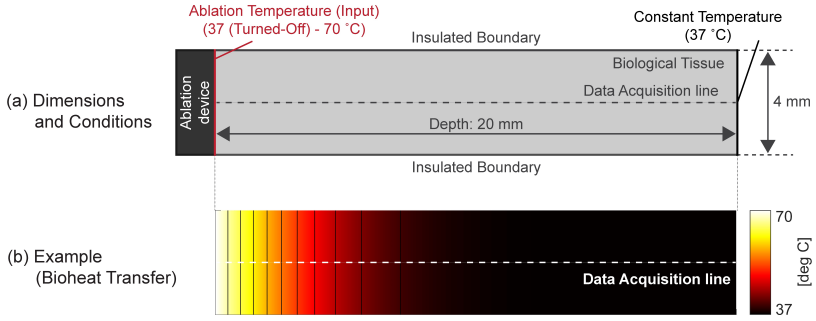

Fig. 4. Defined FEM environment; (a) Geometries and boundary conditions, (b) Example of the heat transfer.

F. Temperature Safety Feature

For the demonstration of the desired automated safety stop, a simple algorithm is implemented as a controller. The algorithm considers the safety temperature limit, T_{limit}, with the safety buffer, δT_{buffer}, and terminates ablation when the following condition is satisfied:

$$T_{\text{est}}[k] \geq T_{\text{limit}} - \delta T_{\text{buffer}} \tag{6}$$

where, $T_{\text{est}}[k]$ is the estimated tissue temperature at step k.

G. Learning Dataset & Training

The learning dataset was generated in the FEM simulation environment. Ablation is initiated at 70 °C and turned off (37 °C) at step k_{drop} ($k_{\text{drop}} = 1, 2, ..., 500$); therefore, the dataset contains 500 episodes in total. In each simulation, ablation temperature, the resulting tissue temperature, and CEM were recorded throughout the simulation time, T_{duration} along the Data Acquisition line.

The initial training was conducted over 200 epochs, followed by 65 rounds of additional training, each lasting 100 epochs. Adam optimizer was used throughout the entire process. This repeated training approach was chosen to take advantage of Adam's initialization feature at the start of each learning cycle.

III. RESULTS

To evaluate the performance of each component in the developed architecture, the evaluation is divided into several parts. Once the basic performance is evaluated, the developed safety feature is demonstrated as an example.

In this study, the estimation errors are evaluated mainly for the duration until the ablation is terminated (100 seconds) because the estimation performance in this time window is critical for the desired safety feature.

A. NSS Performance in Approximating FEM

For the evaluation of the approximation capability of the developed NSS model, the same time-dependent ablation temperature was applied to both the FEM simulation environment and the NSS model after learning the dataset (Fig. 5). To compare each case directly, the ablation temperature is initiated at 70 °C and turned off (37 °C) at 100 seconds throughout this study, and the tissue depth for temperature and CEM is fixed at 5 mm. Note that the EKF is not yet implemented at this point.

With this specific condition, both the approximated tissue temperature and CEM closely match the FEM output except for a certain duration around 100 seconds, when the ablation is turned off. The maximum approximation errors before the termination of ablation are less than 1 °C and around 1 min for the tissue temperature and CEM, respectively. After the termination, the maximum errors are around 2.5 °C and 8 min.

B. Robustness against Modeling Errors

The aim of this section is to evaluate how the implemented EKF can robustly estimate the tissue temperature when the modeling errors are introduced. Since the FEM dataset was

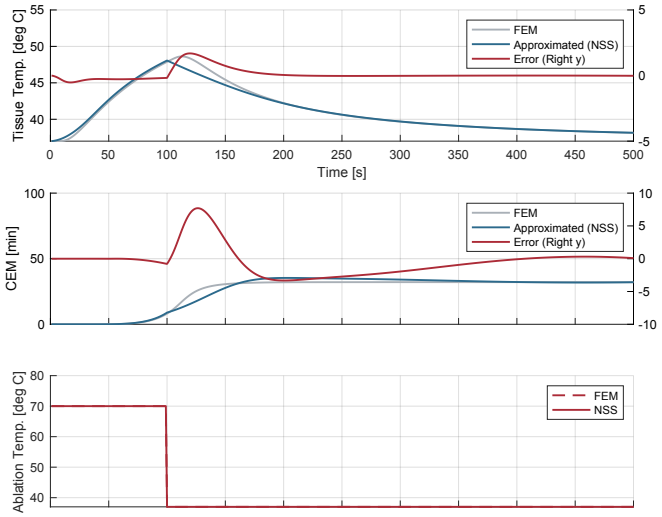

Fig. 5. Approximated FEM simulation by the Neural State Space model.

generated just based on the nominal parameters shown in Table I, the obtained EKF also starts with the nominal models.

1) Bioheat Transfer Model: The bioheat transfer model (Equation 1) considered in this study has three parameters, k, c_p, and ρ. Here, these three parameters were combined and dealt with as the thermal diffusivity, $\alpha(:= k/(\rho c_p))$ [m^2/s].

As the modeling errors, the proportional errors ($\pm$10% and $\pm$20%) of α were applied to the FEM simulation environment, and the EKF took the measured CEM value and the ablation temperature as the output and input, respectively to predict and correct its state estimation (Fig. 6). With these conditions, the maximum estimation error in tissue temperature was around 1 °C.

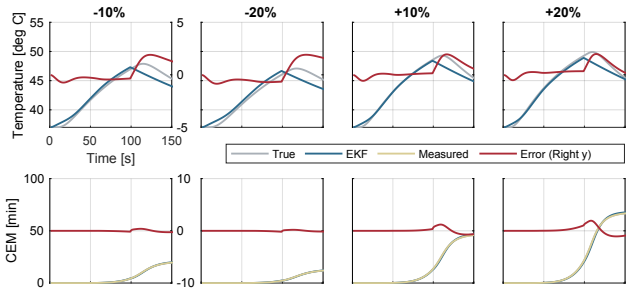

Fig. 6. Robustness against modeling errors in bioheat transfer model.

2) Necrosis Formation Model: To further study the robustness against the modeling errors, the errors were applied to the other model assumed, the necrosis formation model (Equation 2). In this study, the parameter R is selected as it is directly related to the tissue temperature. The proportional errors ($\pm$10% and $\pm$20%) were applied to $R = 0.5$, the nominal value when the tissue temperature is 43 °C or more (Fig. 7). Similar to the case of the bioheat transfer model, it is observed that the maximum estimation error is around 1 °C.

For both modeling errors, the maximum error observed

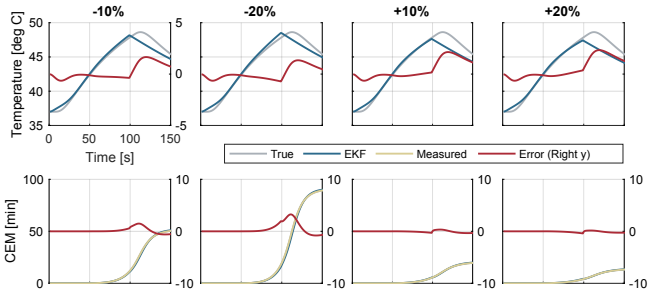

Fig. 7. Robustness against modeling errors in necrosis formation model.

before terminating ablation was around 1 °C, which is less than 5 % of the range of applied ablation temperature (33 °C). Since we aimed to implement the safety feature working with necrosis progression-based feedback control without any additional sensing hardware, it can be concluded that a 5 % estimation error seems acceptable for this application.

C. Robustness against Sensing Errors

Since it is envisioned that the developed tissue temperature estimation scheme will be applied to a variety of modalities sensing necrosis formation, investigating the estimation robustness against the errors happening in the necrosis sensing process should be valuable. Random and shifted sensing errors were simulated and applied separately to decompose the influence of each type of sensing error. The amount of the sensing errors were $\pm$20 and $\pm$40 % for the random noise, and $\pm$20 and $\pm$50 % for the shifted noise (Fig. 8). For the random noise, although some oscillation is observed in the estimation, the move mean of the estimation looks consistent in the cases of $\pm$20 and $\pm$40 %, which is reasonable considering the characteristics of the EKF. For the shifted noise, it is observed that the estimation error gets larger for the amount of the shifted error, but the maximum error observed before terminating ablation was still around 1 °C even with the $\pm$50 % error.

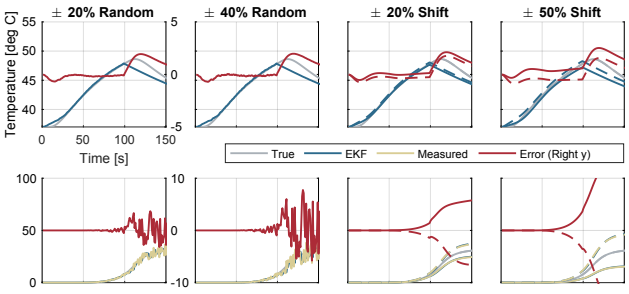

Fig. 8. Robustness against necrosis sensing errors (for shifted error; Solid lines: Negative, Dashed lines: Positive).

D. Control Demonstration (Safety Feature)

Lastly, we performed a demonstration to confirm how the implemented tissue temperature estimation works to realize the desired safety feature, a set of parameters including both the modeling and sensing errors was assumed and implemented the automated safety feature as defined in Section

II-F. The assumed error parameters in this demonstration are summarized in Table II.

TABLE II

ERROR PARAMETERS FOR SAFETY FEATURE DEMONSTRATION

Symbols	Description	Value [unit]
T_{limit}	Safety temperature limit	46 [°C]
δT_{buffer}	Safety buffer	1.5 [°C]
$\delta\alpha_{\text{error}}$	Modeling error in α	+20 [%]
δR_{error}	Modeling error in R (≥ 43 °C)	−20 [%]
N_{rand}	Random necrosis sensing noise (range)	±20 [%]

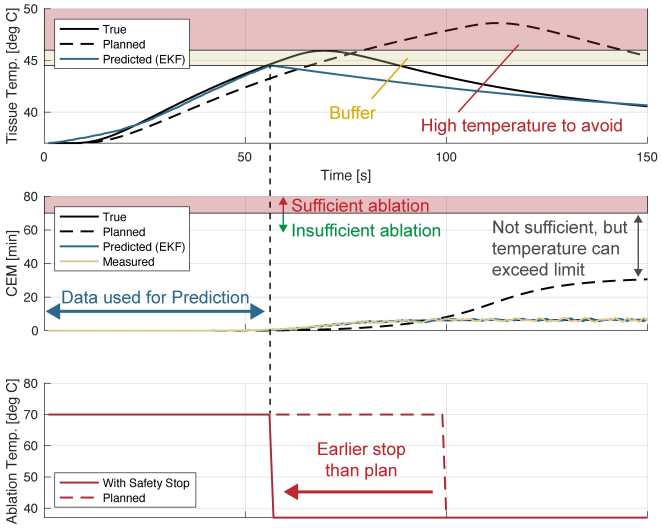

Fig. 9. Demonstration of desired temperature safety feature.

IV. DISCUSSIONS

One thing to be noted first is that the demonstration in Fig. 9 well exemplifies the situation where the tissue temperature exceeds a safety temperature limitation even far before the tissue is ablated. This corroborates our concern about the potential overheating when only relying on necrosis sensing, supporting the importance of adding the temperature estimation mechanism to necrosis sensing.

As the next step of this study, we plan to design a model predictive control (MPC) architecture with the NSS model and the state estimation for ablation control. As illustrated in the results, the tissue temperature does not immediately drop when ablation is terminated, which is due to the thermal inertia of the tissue. This effect can result in overheating and continue to form necrosis even after the ablation is terminated. Thus, the introduction of MPC is expected to allow clinicians to deal with the dynamics of ablation therapy more effectively. In fact, the safety buffer δT_{buffer} used in the demonstration was selected try-and-error basis. The planned extension to MPC is expected to provide a more systematic way to determine these parameters. Another potential improvement is to use the Physics Informed Neural Networks (PINNs) [35], which can potentially provide better approximation performance than the MLP used in this study.

Although the evaluation in this study demonstrated the feasibility of the proposed approach, there are several limitations to be listed and remaining work to do. First, the evaluation was performed only in the simulation environment. The architecture needs to be investigated in the experimental setup using actual biological tissue. If the experiment reveals any higher nonlinearity or unexpected type of noise, using other state estimation algorithms such as the UKF and the PF would be an option to consider. Second, the NSS model was prepared based on the FEM dataset with nominal parameters and the learning dataset only assumed the simple ablation temperature profiles. Also, the neural network structure itself was not optimized in this study. To pursue better estimation performance, the optimization of the neural network structure and the learning process should be optimized. The limited variety of parameter values investigated in this study is another limitation. For example, the tissue depth for the temperature and CEM was fixed at 5 mm in this study. Since it is easily expected that the performance of the developed architecture can be influenced by the tissue depth, the influence of the tissue depth should also be investigated.

Lastly, as this proposed architecture is based on the model approximation with NSS, the same architecture is expected to be generalized to other medical procedures, which would involve high nonlinearity and patient/environment-specific physics, and even to procedures having no reliable theoretical models. One of the candidates would be drug delivery control, especially estimating the concentration of a drug at a specific location inside the body. In the cases where any theoretical models are not available, the NSS model is expected to be prepared through the learning of the actual clinical dataset, which can potentially provide significant flexibility to this approach and it is even possible that the NSS trained with the actual clinical dataset provides better performance than the theoretical models.

V. CONCLUSIONS

In this study, we aimed to propose a necrosis progression-based tissue temperature estimation technique either as an independent estimator or a complimentary estimation component for robustness if other primary thermometers are available. The estimator consists of the NSS model and the EKF, and it does not require any additional sensing hardware. The robustness of the estimation scheme against modeling and sensing errors was evaluated, and the example case of the desired safety feature was demonstrated. Future work should focus on further validation of the scheme in experimental setups using actual biological tissue and the extension of this architecture to MPC-based ablation control to deal with thermal inertia. Additionally, the proposed architecture can be extended to other medical procedures that involve high nonlinearity and patient/environment-specific physics, providing flexibility and potential for better performance than theoretical models.

APPENDIX

The 1-minute video of this study is available.

ACKNOWLEDGMENT

This work is supported by grants (DP5OD028162, R01CA166379, R01CA134675, R01EB030539, and

R01DK133717) from the National Institutes of Health. Mr. Ryo Murakami is partly supported by the Nakajima Foundation Scholarship.

DECLARATIONS

ChatGPT, Claude and GitHub Copilot were used for proofreading to enhance readability and eliminate grammatical errors. The authors reviewed and edited the content and take full responsibility for the content of the publication. The authors have no relevant financial or non-financial interests to disclose.

REFERENCES

[1] A. Franzini, S. Moosa, D. Servello, I. Small, F. DiMeco, Z. Xu, W. J. Elias, A. Franzini, and F. Prada, "Ablative brain surgery: an overview," *International Journal of Hyperthermia*, vol. 36, no. 2, pp. 64–80, 2019.

[2] T. Oka, Y. Koyama, K. Tanaka, Y. Hirao, N. Tanaka, M. Okada, I. Yoshimoto, R. Kitagaki, A. Okamura, K. Iwakura *et al.*, "Post-ablation left atrial function impacts long-term recurrence of atrial fibrillation after ablation," *Heart and Vessels*, vol. 37, no. 2, pp. 315–326, 2022.

[3] R. Murakami, S. Mori, and H. K. Zhang, "Intraoperative ablation control based on real-time necrosis monitoring feedback: Numerical evaluation," *Annals of Biomedical Engineering*, pp. 1–14, 2024.

[4] M. G. Van Vledder, E. M. Boctor, L. R. Assumpcao, H. Rivaz, P. Foroughi, G. D. Hager, U. M. Hamper, T. M. Pawlik, and M. A. Choti, "Intra-operative ultrasound elasticity imaging for monitoring of hepatic tumour thermal ablation," *Hpb*, vol. 12, no. 10, pp. 717–723, 2010.

[5] M. Wright, E. Harks, S. Deladi, F. Suijver, M. Barley, A. van Dusschoten, S. Fokkenrood, F. Zuo, F. Sacher, M. Hocini *et al.*, "Real-time lesion assessment using a novel combined ultrasound and radiofrequency ablation catheter," *Heart Rhythm*, vol. 8, no. 2, pp. 304–312, 2011.

[6] C.-Y. Wang, X. Geng, T.-S. Yeh, H.-L. Liu, and P.-H. Tsui, "Monitoring radiofrequency ablation with ultrasound nakagami imaging," *Medical physics*, vol. 40, no. 7, p. 072901, 2013.

[7] R. Bouchard, N. Dana, L. Di Biase, A. Natale, and S. Emelianov, "Photoacoustic characterization of radiofrequency ablation lesions," in *Photons Plus Ultrasound: Imaging and Sensing 2012*, vol. 8223. SPIE, 2012, pp. 682–687.

[8] N. Dana, L. Di Biase, A. Natale, S. Emelianov, and R. Bouchard, "In vitro photoacoustic visualization of myocardial ablation lesions," *Heart Rhythm*, vol. 11, no. 1, pp. 150–157, 2014.

[9] S. Gao, H. Ashikaga, T. Mansi, H. R. Halperin, and H. K. Zhang, "Photoacoustic necrotic region mapping for radiofrequency ablation guidance," in *2021 IEEE International Ultrasonics Symposium (IUS)*. IEEE, 2021, pp. 1–4.

[10] L. Grecu, "Cardiac tamponade," *International Anesthesiology Clinics*, vol. 50, no. 2, pp. 59–77, 2012.

[11] J. Seiler, K. C. Roberts-Thomson, J.-M. Raymond, J. Vest, E. Delacretaz, and W. G. Stevenson, "Steam pops during irrigated radiofrequency ablation: feasibility of impedance monitoring for prevention," *Heart Rhythm*, vol. 5, no. 10, pp. 1411–1416, 2008.

[12] K. Tsutsui, H. Mori, D. Kawano, N. Tanaka, Y. Ikeda, N. Sumitomo, S. Iwanaga, S. Nakano, T. Muramatsu, K. Matsumoto *et al.*, "Ablation characteristics and incidence of steam pops with a novel, surface temperature-controlled ablation system in an ex vivo experimental model," *Pacing and Clinical Electrophysiology*, vol. 45, no. 12, pp. 1390–1400, 2022.

[13] D. J. Curry, A. Gowda, R. J. McNichols, and A. A. Wilfong, "Mr-guided stereotactic laser ablation of epileptogenic foci in children," *Epilepsy & Behavior*, vol. 24, no. 4, pp. 408–414, 2012.

[14] N. V. Tsekos, A. Khanicheh, E. Christoforou, and C. Mavroidis, "Magnetic resonance–compatible robotic and mechatronics systems for image-guided interventions and rehabilitation: a review study," *Annu. Rev. Biomed. Eng.*, vol. 9, pp. 351–387, 2007.

[15] E. Leshem, I. Zilberman, M. Barkagan, A. Shapira-Daniels, J. Sroubek, A. Govari, A. E. Buxton, and E. Anter, "Temperature-controlled radiofrequency ablation using irrigated catheters: maximizing ventricular lesion dimensions while reducing steam-pop formation," *Clinical Electrophysiology*, vol. 6, no. 1, pp. 83–93, 2020.

[16] P. R. Childs, J. Greenwood, and C. Long, "Review of temperature measurement," *Review of scientific instruments*, vol. 71, no. 8, pp. 2959–2978, 2000.

[17] J. Yao, H. Ke, S. Tai, Y. Zhou, and L. V. Wang, "Absolute photoacoustic thermometry in deep tissue," *Optics letters*, vol. 38, no. 24, pp. 5228–5231, 2013.

[18] Y. Liao, X. Jian, F. Dong, and Y. Cui, "Dual-wavelengths photoacoustic temperature measurement," in *Second International Conference on Photonics and Optical Engineering*, vol. 10256. SPIE, 2017, pp. 296–301.

[19] X. Jian, N. Wang, C. Yang, Z. Han, J. Xu, Z. Li, Y. Cui, and F. Dong, "Multiwavelength photoacoustic temperature measurement with phantom and ex-vivo tissue," *Optics Communications*, vol. 457, p. 124724, 2020.

[20] R. M. Arthur, W. Straube, J. Trobaugh, and E. Moros, "Non-invasive estimation of hyperthermia temperatures with ultrasound," *International journal of hyperthermia*, vol. 21, no. 6, pp. 589–600, 2005.

[21] J. Seo, S. K. Kim, Y.-s. Kim, K. Choi, D. G. Kong, and W.-C. Bang, "Motion compensation for ultrasound thermal imaging using motion-mapped reference model: An in vivo mouse study," *IEEE Transactions on Biomedical Engineering*, vol. 61, no. 11, pp. 2669–2678, 2014.

[22] Z. Chen and R. Barbieri, *A dynamic point process framework for assessing heartbeat dynamics and cardiovascular functions*. Cambridge University Press, 2015, pp. 302–329.

[23] W. Wu and S. Liu, *Neural decoding in motor cortex using state space models with hidden states*. Cambridge University Press, 2015, pp. 207–230.

[24] G. Pennati, C. Corsini, T.-Y. Hsia, F. Migliavacca, and M. of Congenital Hearts Alliance (MOCHA) Investigators, "Computational fluid dynamics models and congenital heart diseases," *Frontiers in pediatrics*, vol. 1, p. 4, 2013.

[25] J. Zamarreno, P. Vega, L. Garcıa, and M. Francisco, "State-space neural network for modelling, prediction and control," *Control Engineering Practice*, vol. 8, no. 9, pp. 1063–1075, 2000.

[26] I. V. Stelzer, J. Kager, and C. Herwig, "Comparison of particle filter and extended kalman filter algorithms for monitoring of bioprocesses," in *Computer Aided Chemical Engineering*. Elsevier, 2017, vol. 40, pp. 1483–1488.

[27] H. H. Pennes, "Analysis of tissue and arterial blood temperatures in the resting human forearm," *Journal of applied physiology*, vol. 1, no. 2, pp. 93–122, 1948.

[28] K. Y. Gandomi, P. A. Carvalho, M. Tarasek, E. W. Fiveland, C. Bhushan, E. Williams, P. Neubauer, Z. Zhao, J. Pilitsis, D. Yeo *et al.*, "Modeling of interstitial ultrasound ablation for continuous applicator rotation with mr validation," *IEEE Transactions on Biomedical Engineering*, vol. 68, no. 6, pp. 1838–1846, 2020.

[29] M. W. Dewhirst, B. Viglianti, M. Lora-Michiels, M. Hanson, and P. Hoopes, "Basic principles of thermal dosimetry and thermal thresholds for tissue damage from hyperthermia," *International journal of hyperthermia*, vol. 19, no. 3, pp. 267–294, 2003.

[30] Z. Campwala, B. Szewczyk, T. Maietta, R. Trowbridge, M. Tarasek, C. Bhushan, E. Fiveland, G. Ghoshal, T. Heffter, K. Gandomi *et al.*, "Predicting ablation zones with multislice volumetric 2-d magnetic resonance thermal imaging," *International Journal of Hyperthermia*, vol. 38, no. 1, pp. 907–915, 2021.

[31] R. Dhaouadi, N. Mohan, and L. Norum, "Design and implementation of an extended kalman filter for the state estimation of a permanent magnet synchronous motor," *IEEE Transactions on Power Electronics*, vol. 6, no. 3, pp. 491–497, 1991.

[32] S. J. Julier and J. K. Uhlmann, "Unscented filtering and nonlinear estimation," *Proceedings of the IEEE*, vol. 92, no. 3, pp. 401–422, 2004.

[33] T. Chen, J. Morris, and E. Martin, "Particle filters for state and parameter estimation in batch processes," *Journal of process control*, vol. 15, no. 6, pp. 665–673, 2005.

[34] P. A. Hasgall, F. Di Gennaro, C. Baumgartner, E. Neufeld, B. Lloyd, M. Gosselin, D. Payne, A. Klingenböck, and N. Kuster, "It'is database for thermal and electromagnetic parameters of biological tissues," *Version 4.1*.

[35] S. L. Brunton and J. N. Kutz, *Data-driven science and engineering: Machine learning, dynamical systems, and control*. Cambridge University Press, 2022.